Optically driven fluid flow along arbitrary microscale patterns using thermoviscous expansion

Franz M. Weinert and Dieter Braun[a)]
Systems Biophysics, Functional NanoSystems, Center for Nanoscience (CENS), Department of Physics, Ludwig-Maximilians University Munich, Amalienstr. 54, 80799 Munich, Germany

(Received 25 June 2008; accepted 8 October 2008; published online 25 November 2008)

We show how fluid can be moved by a laser scanning microscope. Selected parts of a fluid film are pumped along the path of a moving warm spot which is generated by the repetitive motion of an infrared laser focus. With this technique, we remotely drive arbitrary two-dimensional fluid flow patterns with a resolution of 2 μm. Pump speeds of 150 μm/s are reached in water with a maximal temperature increase in the local spot of 10 K. Various experiments confirm that the fluid motion results from the dynamic thermal expansion in a gradient of viscosity. The viscosity in the spot is reduced by its enhanced temperature. This leads to a broken symmetry between thermal expansion and thermal contraction in the front and the wake of the spot. As result the fluid moves opposite to the spot direction due to both the asymmetric thermal expansion in the spot front and the asymmetric thermal contraction in its wake. We derive an analytical expression for the fluid speed from the Navier–Stokes equations. Its predictions are experimentally confirmed without fitting parameters under a number of different conditions. In water, this nonlinearity leads to a fluid step of <100 nm for each passage of the spot. Since the spot movement can be repeated in the kilohertz regime, fluid speeds can exceed 100 μm/s. Using this technique, we pump nanoparticles over millimeters through a gel. An all-optical creation of a dilution series of DNA and biomolecules by aliquotation and mixing is demonstrated for fluids sandwiched between untreated and unstructured, disposable microscope cover slips. The shown optical remote control of fluid flow expands the microfluidic paradigm into previously inaccessible regimes of tiny volumes, closed flow paths, fast switching between flow patterns, and remote fluid control under extreme fluid conditions. © *2008 American Institute of Physics*. [DOI: 10.1063/1.3026526]

I. INTRODUCTION

The defined control of fluid flow on the microscale is the basis for several applications in chemistry and biology[1–5] and plays an important role in scaling biosensing applications down to the scale of single cells. The aim is to find a defined control of volumes comparable to the size of biological systems. This miniaturization is expected to shorten the time of the experiment, to enhance the signal to noise ratio of detection and to reduce the overall consumption of chemicals. In the past, several ways to remotely switch valves in micromanufactured channels for the control of fluid flow in channels have been explored.[6–10] Optical methods have been investigated to move covered liquid droplets[11,12] or to drive liquid flow by holographically induced vortex flows near trapped particles.[13] Lithographic surface patterning is used to induce droplet movement by thermocapillary actuation[14] or surface acoustic waves.[15] Here we propose an optical remote driving and random access control of two-dimensional liquids without surface patterning or the usage of special substrates.

Today, pressure is the dominating paradigm to drive flow along microscale channels. However, its control suffers from hysteresis effects and requires macroscale connections to outside pumps and controllers. An interesting aspect of the presented method is its complementary approach as compared to contemporary microfluidics. Our technique neither requires walls to define the fluid motion nor needs channels with external pressure control to drive the fluid flow by pressure and does not rely on valves to switch between pump paths. We drive fluids highly locally, contact-free, and all optical. This allows to move fluids along paths which are arbitrarily defined without channel walls. We believe that the high reproducibility of optical techniques and the fact that the pump velocity enhances for thinner fluid films open a range of unexpected applications of the approach and point towards reliable nanofluidic designs.

The ability to remotely control matter with light has unique advantages. In many fields of physics and biology, optical control of matter is used due to its versatility and precision and has had a major impact on experimental methods. For example, optical traps allowed to cool and isolate single atoms in vacuum in a wide variety of geometries. Furthermore, optical tweezers[16–18] have been employed to grab and move objects on the microscale under physiological conditions. In the reported experiments, we expand the optical control paradigm to the continuum mechanics regime. Instead of controlling the movement of objects with optical contrast, we describe the arbitrary optical control of a homogeneous fluid film. We can realize arbitrary solutions of the

[a)]Author to whom correspondence should be addressed. Electronic mail: dieter.braun@physik.lmu.de.

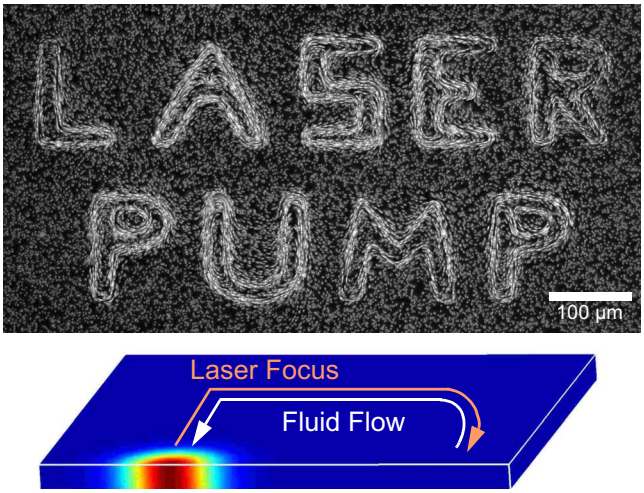

FIG. 1. (Color online) Pumping water optically along arbitrary patterns. Fluid flow along the letters "LASER PUMP" is driven by dynamically heating a thin fluid film with a laser scanning microscope. As seen, complex flow patterns are easily accomplished. No channels restrict the fluid flow. Local pumping of the fluid film is the result of thermoviscous fluid movements for each passage of the laser focus. We visualize the water flow by fluorescent tracer particles. Movies of flow patterns can be found in the supplementary materials section.

two-dimensional Navier–Stokes equation with a resolution of a few micrometers and velocities on the order of 100 μm/s.

Using the nonlinear effect described here, we can, for example, move water along the letters "LASER PUMP" without lateral walls to guide the flow (Fig. 1). In the example, we sandwich a 10 μm thin sheet of water between glass slides and move an infrared laser focus along the letters with a laser scanning microscope. The water is locally heated by direct absorption of the laser irradiation. The spot movement along the letters is repeated in the kilohertz regime. As result, the fluid flows the reverse path of warm spot movement. In the following we describe the theoretical basis of the effect, derive an expression for the pump velocity, test the expression in various experiments, and end with discussing the prospects and limitations of the approach.

II. EXPERIMENT

A. Optical setup and imaging

The infrared laser scanning microscope is operated with a fiber laser (RLD-5-1455, IPGLaser, 5 W) at wavelength of 1455 nm, collimated to a $1/e^2$ diameter of 1.5 mm (F240FC-1550, Thorlabs). Water absorbs this wavelength strongly with an attenuation length of 305 μm. The absorbed light power ranged in intensity from 1 to 100 mW. An acousto-optical deflector (Pegasus Optik, AA.DTS.XY.100) modulated and moved the laser spot, which was focused into the fluid chamber from below with a long distance lens [Thorlabs, C240TM-C, focus length $f=8$ mm, numerical aperture NA=0.5, $NA_{eff}=0.07$]. For experiments with small spot diameters (Fig. 5) we focused the beam using a lens with high NA (Thorlabs, C570TM-C, $f=2.84$ mm, $NA_{eff}=0.2$). Imaging was provided by an upright fluorescence microscope (Zeiss, Axiotech Vario) from the top. For illumination, a green light emitting diode (LXHL-LX5C, Luxeon) was driven with a current source (LD-3565, ILX Lightwave, modulation bandwidth of 100 kHz).

Flow velocities were measured by tracing 80 pM of green fluorescent 1 μm diameter silica microspheres (PSi-G1.0, Kisker, Germany) which showed negligible optical trapping at the used focus size. This was tested with heavy water with 100-fold lower light absorption, which should show similar optical trapping. Under otherwise identical conditions, no optical trapping and no movement of the particles were found, indicating that optical trapping or other optical forces due to the focused laser light play no role. Optical trapping would move the tracer particles towards the laser spot movement, opposite to the observed flow direction. Tracking resolution was typically 100 nm. We used a circular pump geometry with a radius of 60 μm to measure the velocities.

Temperatures were imaged using 50 μM of the fluorescent dye 2′,7′-bis(carboxy-ethyl)-5(6)-carboxyfluorescein (Molecular Probes) in 10 mM tris(hydroxymethyl) aminomethane hydrochloride buffer at *p*H 7.8. The fluorescence depends on temperature and was translated to chamber-averaged temperatures with a sensitivity of −0.013/K.[19] The shape and temperature of the moving spot were imaged stroboscopically with a 10 μs long rectangular light pulse each time the laser spot passed by. The flow was imaged by averaging over subsequent image differences. The tracer particles were solved in 75% (v/v) glycerol/water to enhance the flow contrast by suppressing diffusion.

B. Chambers and light driven microfluidics

If not indicated explicitly, the chamber thickness was 6.5 μm. The chamber thickness was measured by focusing the top and the bottom of the chamber with a calibrated z drive. For Fig. 8, a 45 °C warm, 2 μl drop of low melting agarose gel (A3038, Roth Laborbedarf) was sandwiched between two glass slides. After gelation by cooling to room temperature, a 120 nM solution of 40 nm beads in water (F8795, Molecular Probes) were pipetted at the edge of the cover slide. Capillary forces pulled the liquid inside and formed an interface towards the gel. The chamber height was 10 μm. The gel was initially molten with a low repetition rate ($f=1$ Hz), while the fluid was pumped along the trace at $f=50$ Hz.

In Fig. 9, the preparation for the gel interface additionally required to further suppress the diffusion of the small biomolecules by the addition of 66% saccharose to the gel.

For Fig. 10, two droplets of 2% low melting agarose gel in 10 mM TRIS buffer together with 60 vol % of saccharose were put on a 45 °C warm silicon wafer. The silicon wafer was polished on both sides and had 1000 nm of SiO_2 with 40 nm CrNi (20% Cr and 80% Ni) evaporated on top which increased the infrared absorption 15-fold. The infrared laser was fed through the silicon chip which is transparent at this wavelength. After covering the liquid gel with a glass slide, both fluids spread into the air-filled chamber space, forming an interface between each other. In the gel at the bottom of the image, 100 μM of a 30 kDa dextran with a fluorescein

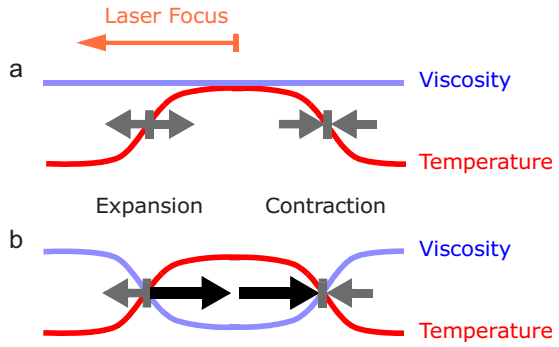

FIG. 2. (Color online) Basic mechanism for pumping fluid with a moving laser focus. (a) A warm temperature spot moving to the left generates thermal expansion in its front and contraction in its wake, shown with dark gray arrows. These local fluid movements cancel out each other at constant viscosity. (b) The temperature dependency of the fluid's viscosity breaks this symmetry and results in a net liquid flow to the right (black arrows). If the fluid expands upon heating and shows a decreased viscosity, this flow is directed against the movement of the spot as indicated by the black arrows.

dye (D1844, Molecular Probes) was dissolved. Before the fluid was pumped with repetition rate $f=3$ kHz, the spot was moved at $f=0.5$ kHz for 0.8 s to melt the pump channels into the gel. The gelation is kinetically hindered and subsequent pumping can be performed at reduced temperature in the premolten, stable channel structures. The overall protocol time was 15 s.

C. Finite element calculations

Finite element calculations were performed using the industrial Comsol FEMLAB 3.1 solver. The Navier–Stokes equations were calculated in various geometrical settings and different stages of approximation, typically in the comoving frame of the warm spot. The simulation files are provided as supplemental material.[20]

III. RESULTS AND DISCUSSION

A. Basic mechanism

We sketch the basic physical principles in Fig. 2 before we enter a detailed theoretical treatment. Let us consider a moving warm spot of enhanced temperature that moves to the left [Fig. 2(a), red]. At its front, the fluid is heated. In its wake it cools down again. The heating triggers thermal expansion and thus a diverging fluid flow in the front of the spot (gray arrows). The fluid contracts again upon cooling in the wake of the spot. For a constant viscosity, both movements are antisymmetric and cancel out each other.[21] However, since the viscosity of the fluid typically drops with temperature, the expansion and contraction movements take place in a gradient of viscosity [Fig. 2(b), blue] and lead to a net fluid movement to the right. Qualitatively, the net flow results from the fact that thermal expansion feels less friction to the solid walls when it moves fluid towards than away from the spot. Due to the sign change of the viscosity gradient at the front as compared to the wake of the spot, we find a net fluid movement to the right from both expansion and contraction (black arrows).

For extended thermal waves we have discussed a similar effect in the past.[22] However, here we found that the movement of a single focus spot gives a much simpler implementation of the effect. Furthermore, with a single spot we can reach pump velocities exceeding 150 μm/s for maximal spot temperatures of $\Delta T_0=10$ K above the background chamber temperature. Under these conditions, thermal waves could only trigger a fluid flow of 5 μm/s along a circular geometry.

B. Analytical solution

The above qualitative illustration can be derived quantitatively from first principles. Let us consider the stationary solutions of the Navier–Stokes equations:

$$-\rho\frac{\partial \mathbf{u}}{\partial t}-\rho(\mathbf{u}\cdot\nabla)\mathbf{u}+\nabla\cdot\eta[\nabla\mathbf{u}+(\nabla\mathbf{u})^T]=\nabla p,$$

$$\frac{\partial \rho}{\partial t}+\nabla\cdot(\rho\mathbf{u})=0, \tag{1}$$

in the moving frame of the temperature spot. Variables are the fluid velocity $\mathbf{u}=(u,v,w)$ for the x, y, and z directions. The velocity of the warm spot along the x direction is denoted by u_{spot}, the pressure by p, density by ρ, and viscosity by η. We describe the fluid flow in the frame of the temperature spot which moves along the x axis with a temperature increase of $\Delta T=\Delta T(x-tu_{\text{spot}},y)$. Due to stationarity, the time derivatives $\partial u/\partial t$, $\partial v/\partial t$, and $\partial\rho/\partial t$ are replaced by convective terms $-u_{\text{spot}}u_x$, $-u_{\text{spot}}v_x$, and $-u_{\text{spot}}\rho_x$ in the moving frame. Furthermore the lubrication approximation for thin films is used as follows. The velocities u and v describe the average film velocity along the x and y axes. Assuming a parabolic fluid profile, friction terms $12u\eta/d^2$ and $12v\eta/d^2$ arise from the integration over the film in the z direction with d being the fluid thickness. With the nomenclature $u_x=\partial u/\partial x$, the momentum balance of the Navier–Stokes equations becomes

$$\rho u_{\text{spot}}u_x-\rho(uu_x+vu_y)=\frac{\partial}{\partial x}[p-2\eta u_x]-\frac{\partial}{\partial y}[\eta(u_y+v_x)]+12(u+u_{\text{spot}})\eta/d^2,$$

$$\rho u_{\text{spot}}v_x-\rho(uv_x+vv_y)=-\frac{\partial}{\partial x}[\eta(v_x+u_y)]+\frac{\partial}{\partial y}[p-2\eta v_y]+12v\eta/d^2. \tag{2}$$

The inertial terms on the left side of Eq. (2) are negligible due to a small Reynolds number of typically around Re=0.02. One can assume that thermal expansion is equilibrated since the speed of sound in water (1400 m/s) is much faster than the movement of the laser spot ($u_{\text{spot}}=0.2$ m/s). As result, we do not explicitly implement the expansion dynamics with an equation of state for water but we insert the change in density directly into the continuity equation using $\rho=\rho_0(1-\alpha\Delta T)$ with the thermal expansion coefficient $\alpha=(1/\rho)(\partial\rho/\partial T)$. Inserting the convective terms and the thermal expansion term $\rho_x(u+u_{\text{spot}})=\rho_0\alpha u_{\text{spot}}\Delta T_x+\rho_x u_{\text{spot}}$ we find for the continuity equation

$$\rho(u_x+v_y)+\rho_0\alpha u_{\text{spot}}\Delta T_x+\rho_y v=0. \tag{3}$$

We assume that the temperature spot is wider than the thickness of the water film ($d=10\ \mu$m). Thus friction within the fluid layer becomes smaller than the friction towards the boundaries of the film: $\eta v_{xx} \ll 12 v \eta / d^2$. As seen above, the change in density only plays a role in the $\rho_x u$ term. For all other terms, we keep the density constant and substitute with $\rho \rightarrow \rho_0$. We checked numerically that the dynamics in the y direction does not contribute to the final pump velocity. Since the fluid flow from thermal expansion is much slower than the spot velocity ($v \ll u_{\text{spot}}$) we can drop the term $\rho_y v$. We can now transfer back to the resting frame of reference of the chamber walls with $u+u_{\text{spot}} \rightarrow u$. As a result, Eqs. (1) and (2) are greatly simplified mostly due to the treatment with low Reynolds numbers:

$$p_x + 12u\eta/d^2 = 0,$$

$$p_y + 12v\eta/d^2 = 0,$$

$$u_x + v_y + \alpha u_{\text{spot}} \Delta T_x = 0. \tag{4}$$

To apply the identity $p_{xy}=p_{yx}$, we combine the two top momentum equations by subtracting the y derivative of the first from the x derivative of the second, leading to $(u_y - v_x)\eta + u\eta_y - v\eta_x = 0$. No net pumping perpendicular to the spot movement (y direction) is expected since thermal expansion and thermal contraction are located in an equal gradient of the viscosity. Only along the x direction thermal expansion faces a gradient of viscosity which is inverted upon later thermal contraction. We thus drop all terms with velocity v and find

$$u_y \eta + u \eta_y = 0,$$

$$u_x + \alpha u_{\text{spot}} \Delta T_x = 0. \tag{5}$$

We make the viscosity temperature dependent with $\eta = \eta_0(1-\beta\Delta T)$ and temperature coefficient $\beta = (1/\eta)(\partial\eta/\partial T)$. The second line can be readily integrated along x and inserted into the first, leading to $u_y + \alpha\beta u_{\text{spot}} \Delta T \Delta T_y = 0$ which is again readily integrated along y to yield

$$u = -\frac{\alpha\beta}{2} u_{\text{spot}} \Delta T^2. \tag{6}$$

We move the spot repeatedly over the same location with frequency f. Each passage of the spot makes the fluid center shift by Δx. This shift can be inferred from the integration of the peak fluid velocity $3u/2$ over time for a full passage of the warm spot. The peak fluid velocities can be inferred from average fluid velocities by multiplying with a factor of $3/2$ due to the parabolic flow profile along the z direction:

$$u_{\text{flow}} = f\Delta x = \frac{3f}{2}\int_{-\infty}^{\infty} (u + u_{\text{spot}})dt = \frac{3f}{2}\int_{-\infty}^{\infty} \frac{u + u_{\text{spot}}}{u_{\text{spot}}} dx. \tag{7}$$

The time integral is transformed to the space coordinates of a fixed frame of reference with the substitution $dx/dt = u_{\text{spot}}$. For thermal spot velocities slower than the thermal equilibration time, dynamic heating and cooling do not deform the temperature spot geometry and we can assume a Gaussian temperature distribution $\Delta T = \Delta T_0(y)\exp[-(x-u_{\text{spot}}t)^2/(2b^2)]$ with spot width b. Only for faster velocities do we find experimentally by imaging the temperature spot with stroboscopic illumination that the lagging cooling in the wake of the spot creates an asymmetric temperature spot. In these cases, adapted temperature distributions were used to describe the experimental results. Notably, the temperature changes by less than 15% along the z axis according to steady state calculations of the heat equation with the respective water and glass materials. Therefore, although a drop in the z direction towards the chambers is necessary to cool the water, it has a minor contribution to the resulting pump velocity. For the case of a Gaussian temperature distribution without z dependence, we find a flow velocity of

$$u_{\text{flow}} = -\frac{3\sqrt{\pi}}{4} f\alpha\beta b \Delta T_0^2. \tag{8}$$

For other shapes of the temperature spot, the prefactor from the integration will change. The negative sign indicates that for positive α and β the flow velocity u is directed oppositely to the spot movement. So we have found that pumping is only found for nonzero thermal expansion ($\alpha \neq 0$) and a temperature dependent viscosity ($\beta \neq 0$). The fluid velocity u_{flow} depends linearly on the repetition rate f of the spot movement. It raises quadratically with the applied temperature increase ΔT_0, as expected by combining linear expansion with a linear temperature dependent viscosity. Apparently the thickness of the water film does not enter Eq. (8) which is also found experimentally for small repetition frequencies f. However, only for thin chambers can the temperature spot be moved at high repetition rates f without deformation of the geometry of the temperature field, which makes the method most effective for chamber sizes below about 50 μm.

We insert numbers for water. The thermal parameters at room temperature are $\alpha = 3.3\times10^{-4}/\text{K}$ and $\beta = 0.021/\text{K}$. With a spot frequency of $f=5$ kHz, a width of the temperature spot $b=27\ \mu$m, and a peak temperature $\Delta T_0 = 9$ K, we find from Eq. (8) a peak flow velocity of $u_{\text{flow}} = 100\ \mu\text{m/s}$. We applied the above conditions in an experiment inside a $d=6.5\ \mu$m thin film of water. We find a peak flow velocity of $u_{\text{flow}} = 95\ \mu\text{m/s}$, in good agreement with the theoretical model.

C. Numerical solution

The above analytical solution was checked against the numerical solution of Eqs. (2) and (3) using a commercial finite element solver program (Comsol, FEMLAB) in both three and two dimensions (Fig. 3). The boundary conditions imposed fluid velocity in accordance to the moving frame of reference. From the left ($-x$), the fluid flow is introduced with $u=-u_{\text{spot}}$ and freely flows out of the simulated area on the right side (x) with a pressureless outflow boundary condition. The top ($+y$) and bottom ($-y$) boundaries are kept neutral at a sufficient distance to not hinder the flow dynamics around the spot. Results are plotted by adding the spot velocity u_{spot} to the calculated flow field to show the fluid

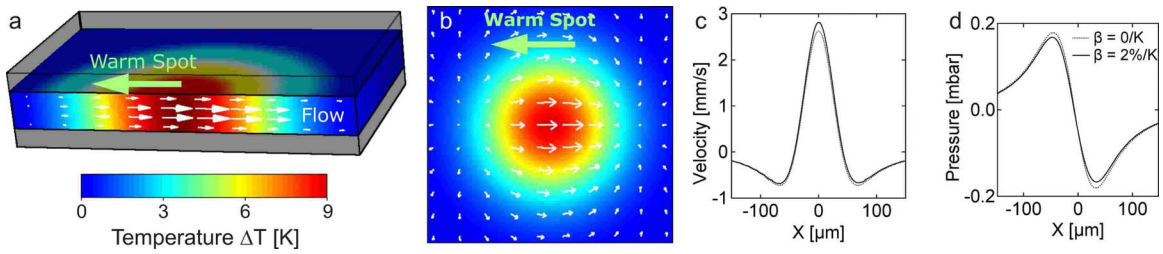

FIG. 3. (Color online) Numerical finite element calculation of thermoviscous pumping. (a) A temperature spot (color coded), is moving to the left and results in an expansion in its front (left) and a contraction in its wake (right). The resulting fluid flow to the right is calculated in three dimensions and indicated by white arrows. The resulting flow has a parabolic flow profile, allowing its description with a thin film approximation. (b) Pumping velocities calculated using the thin film approximation in two dimensions. The average velocity is viewed from top and calculated in the coordinate system of the moving spot. The fluid flow is shown as white arrows, color coded is the temperature $\Delta T(x,y)$. [(c) and (d)] Velocity and pressure profile in the spot along the x-axis. The integral over the velocity is only nonzero for $\beta \neq 0$ due to extended tails in the positive and negative x-directions. The pressure profile is positive in front of the spot as result of the thermal expansion and negative in its wake. Friction reduces for $\beta \neq 0$. Calculations were made using FEMLAB. The simulation files can be found in the supplementary materials.

flow in the resting frame of the chamber. Additional simulation parameters were the density $\rho_0 = 1000\ \mathrm{kg/m^3}$ and the viscosity $\eta_0 = 0.64 \times 10^{-3}$ Pa s for water at room temperature. The numerical calculation allowed to confirm the applied approximations in detail.

The numerical solution for the velocity around the focus is plotted in three dimensions in Fig. 3(a) and in two dimensions in Fig. 3(b). The spot is moving from right to left. In both simulations we find that the fluid expands in the front of the spot and contracts in the tail on the right side of the temperature spot. A parabolic flow profile can be found in the three dimensional solution, confirming the lubrication approximation used in the analytical treatment. As seen by the white arrows, the fluid is pumped across the warm spot by thermal expansion in the front of the spot and thermal contraction in its back. We plot the velocity in the center of the spot along the x axis in Fig. 3(c). Due to large tails of negative velocity for large absolute values of x, the integral over the velocity vanishes if the viscosity is kept constant with $\beta = 0$ (dashed line). This is expected since the simple movement of an expansive spot does not lead to a net fluid movement. Only for temperature dependent viscosity with $\beta \neq 0$ do we find a net movement through the spot. The velocities, however, increase only slightly for $\beta = 0.02\ \mathrm{K^{-1}}$ as plotted by the solid line. This slight increase accounts for all of the found net fluid velocity. Pumping of course does not violate the momentum balance as any momentum required to move the liquid is coupled by the temperature dependent friction to the bordering glass windows. So if pumping is switched on, momentum change of the liquid will result in a tiny momentum transfer to the chamber walls.

In Fig. 3(d) we show the calculated pressure p along the x axis, with $\beta = 0$ (dashed) and $\beta = 0.02\ \mathrm{K^{-1}}$ (solid). For the latter, we find a lower pressure due to a lower friction $F \propto \eta_0(1 - \beta \Delta T)$ in the warm spot to the walls. Since the pump flows are localized to the micrometer-sized temperature spot, the maximal pressure to drive the fluid is below 0.2 mbar for above described parameters in water. This is at least five orders of magnitude below the typical pressure limitations for microfluidics which are on the order of several tens of bars. To calculate a pressure limit, we calculated the deformation for the used 170 μm thin glass material. The pressure needed to bend the glass at the spot to make room for only 10% of the additional volume from a thermal expansion by $\Delta T = 10$ K in a 10 μm chamber amounts to 240 bar (see finite element calculation in the supplementary material[20]). This comparably large pressure limit is mainly the result of the microscale spot area across which the pressure is applied. Notably, this pressure is still well below the internal pressure of water itself. Compressibility models of water typically assume that water becomes compressible upon approaching a pressure of 20 kbar.

The wavelength of the infrared laser used for heating is chosen such that it is absorbed by the water, not by the surrounding glass chamber materials. Therefore, the thermal relaxation of a micrometer thin layer of water bordered by glass windows is below the millisecond time scale. For example, the relaxation time of a 10 μm thin water sheet is on the time scale of 0.1 ms as approximated from thermal diffusion by $\tau = d^2/(\pi^2 \kappa)$ with the thermal diffusivity $\kappa = k/(c_P \rho)$, the thermal conductivity k, the heat capacity c_P, and the density ρ. Thus for spot repetition rates below 1 kHz, a Gaussian temperature profile is a good approximation. Only for faster laser spot movements, the temperature focus shows an asymmetric shape due to a delayed cooling in the tail. As noted before, pump velocities under such asymmetric spot geometries can be equally described by Eq. (8) with an adapted, asymmetric temperature profile.

An asymmetric temperature profile is not necessary to pump the water sheet. One could argue that the laser is deflected by the thermal lensing of the asymmetric spot and as a result, the light transfers momentum due to the deflected beam and pumps the liquid. However, an estimation shows that this effect would be three orders of magnitude smaller than the observed pump velocities. This model would not explain pumping from a symmetric temperature spot or the nonlinear dependence on spot temperature found in the experiments.

D. Experimental tests

We have argued that every passage of the warm spot results in a liquid step Δx opposite to the spot movement direction. The pump speed is therefore expected to increase in a linear fashion with repetition frequency of the laser spot as given by Eq. (8). This behavior was predicted by the

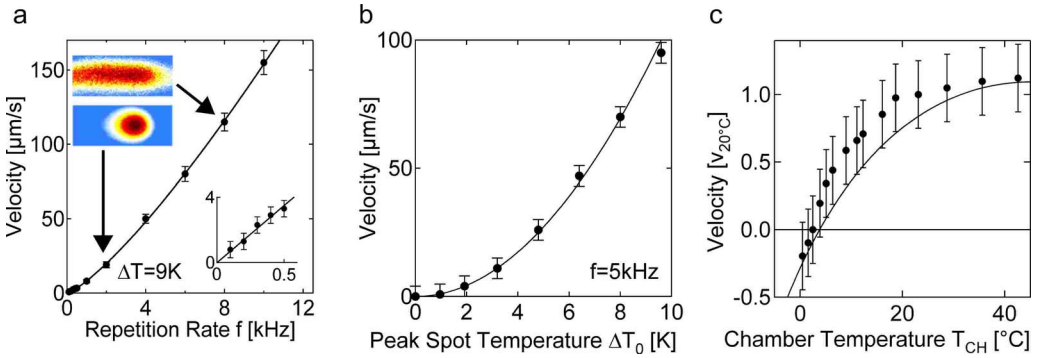

FIG. 4. (Color online) Thermoviscous pumping can be described by the analytical model of Eq. (8). (a) The pump velocity is a linear function of the repetition rate for $f<1$ kHz when the spot geometry remains Gaussian (inset: temperature image). At faster rates, the warm spot becomes elongated due to the finite thermal equilibration time of cooling. Accordingly, the pump velocity is enhanced beyond the linear prediction as the spot width b increases from 10 to 20 μm in the 5 μm thin fluid film. The solid line predicts the pump velocities based on extrapolated temperature profiles for each repetition rate f. (b) The pump velocity rises with the square of the spot temperature, confirming the linear dependence on both the thermal expansion and the temperature dependence of the viscosity. Pump velocities are predicted by Eq. (8) without fitting parameters at a spot width $b=25$ μm. (c) By changing the overall chamber temperature T_{ch}, we can probe the dependence on $\alpha(T_{ch})$ and $\beta(T_{ch})$. For $T_{CH}<4$ °C, the water contracts upon heating. As expected from Eq. (8), pump velocity reverses its direction (solid line). In all plots, error bars show standard errors (s.e.m.) from particle tracking.

theory and verified by measurements in the low frequency regime $f \ll 1$ kHz as shown in the inset of Fig. 4(a). The repetition rate f in this experiment was adjusted by scanning the laser with increased velocity along a fixed circular pump geometry. For slow frequencies, the spot temperature distribution is not deformed from its Gaussian shape. A further increase in the spot velocity results in a considerable elongated temperature spot geometry along the pump direction which increased the pump speed beyond the linear estimate using constant spot width b [Fig. 4(a)]. Examples of spot geometries as measured with stroboscopic temperature imaging are given as color coded insets. Interestingly, the nonlinear pump velocity could still be described when the elongated temperature spot geometry was taken into account with a spatial integral of Eq. (7) for each repetition rate [Fig. 4(a), solid line].

Additional experiments further support the model and the used approximations. The analytical theory predicts a linear response of the pump velocity to both the thermal expansion $\alpha\Delta T_0$ and the change in the temperature dependent viscosity $\beta\Delta T_0$ for a similar shape of the temperature spot. If the spot temperature is increased by enhanced laser power, the pump velocity increases proportionally to ΔT_0^2. The experiments fully confirmed this parabolic dependence as shown in Fig. 4(b). The solid line results from Eq. (8) without additional fitting parameters and matches the experimental data within the error bars.

We test the proportionality to the parameters α and β by changing the ambient temperature T_{ch} of the chamber. In Fig. 4(c) we changed T_{ch} by cooling the microscope stage with an external heat bath. The experiments reveal a reversal of the pump direction at fluid temperatures below 4 °C. We attribute this reversal to the sign change of the volume expansion coefficient α. The theoretical expectation of Eq. (8) again fits the experimental pump velocities as plotted against the fluid temperature within the experimental errors.

E. Pump path width

We explored the possible spatial resolution and limitations for the applied pattern shape in a number of experiments which are documented in Figs. 5 and 6. We did not derive an analytical theory for the pump velocity dependence perpendicular to the fluid flow. However, one might expect that also in this direction the velocity profile falls off with the square of the spot temperature. To test this, we independently measured the temperature profile with fluorescence and tracked the particle velocity profiles in a straight flow geometry, shown in Fig. 5(a). We found that the fluid velocity is indeed not proportional to a linear temperature profile (dashed line) but to the significantly sharper square of the temperature focus (solid line). Both profiles are compared with the measured velocities from particle tracking of 1 μm particles shown as black dots. We consequently find that the resolution of pumping is enhanced by a factor of $\sqrt{2}$ due to the quadratic nature of the nonlinear pumping mechanism.

By reducing the focus size, flow patterns on the micrometer scale could be realized. We pumped water along the letters "nim" in a 3 μm thin chamber. The paths have a minimal distance of 8 μm as shown in Fig 5(b). The movement

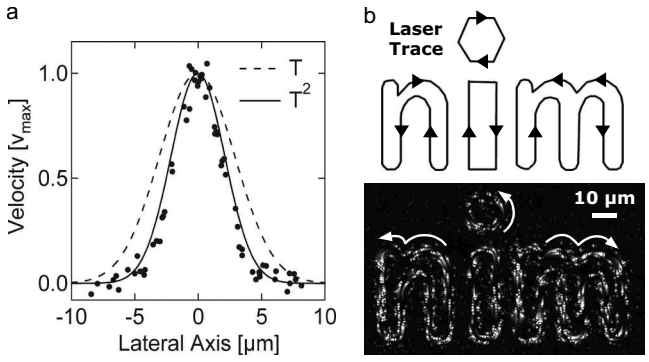

FIG. 5. Controlling fluid flow at optical resolution. (a) The measured lateral temperature of the spot (dashed line) is compared to experimental pump velocities (dots). The width of the pump path follows the significantly sharper ΔT^2-profile (solid line). As result, the resolution of the fluid flow is enhanced by a factor of $\sqrt{2}$. (b) To demonstrate the fluid flow resolution, the laser was moved along the pattern "nim" with minimal path separations of 8 μm. The resulting flow has a resolution of 1.5 μm (standard deviation) at a chamber thickness of 3 μm. As seen, the flow paths do not interfere. The corresponding movie can be found in the supplementary materials section.

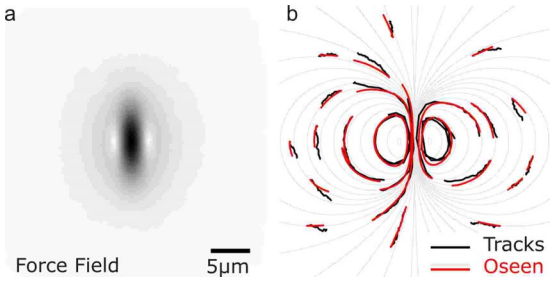

FIG. 6. (Color online) Pumping a finite-sized Oseen tensor. (a) The focus is moved along a short path by a short deflection and a subsequent flyback with the laser switched off, both implemented by the acousto-optical deflector. (b) The generated flow field is inferred from particle tracking of 1 μm beads shown for a recording interval of 7 s (black). Their movement is well described by a finite-sized Oseen tensor (red and gray, see supplementary material). Any solution of the laminar, two-dimensional Navier–Stokes equation can be generated by the superposition of Oseen tensors. Individual pump patterns can be superposed by the laser scanning. As result we can generate arbitrary solutions of the laminar two-dimensional Navier–Stokes equation on the tens of micrometer scale.

of 500 nm tracer particles are shown by the superposition of subsequent frames. We find a flow width with a standard deviation of 1.5 μm. Note that the nearby pump paths showed no interference. It appears that further downscaling of the heating source and the chamber thickness will allow to pump fluids even well below micrometer resolution. The strength of thermal expansion will still allow to drive the fluid flow and as discussed later, pumping even becomes faster in thinner chambers due to the enhanced thermal relaxation speed.

F. Pumping an Oseen tensor

We asked if it is possible to drive any solution of the two-dimensional Navier–Stokes equation in the limit of low Reynolds numbers with micrometer resolution. To test this assertion, we benchmarked the fluid flow with a finite-sized Oseen tensor. An Oseen tensor describes the fluid flow generated from a delta-shaped application of force to the fluid. By showing that we can generate a highly localized flow in the shape of the Oseen tensor, all possible solutions of the two-dimensional Navier–Stokes equation in the limit of laminar flow can be obtained with similar resolution by superposition of the laser scanning patterns. This demonstrates that the presented light driven pump can drive two-dimensional fluids with unprecedented flexibility on the micrometer scale.

We created a finite-size Oseen flow by moving the warm spot unidirectionally over a short distance. The laser is switched off during the flyback motion. We visualized the movement of the fluid with tracer particles and compared their tracks to a finite element calculation of a finite-sized Oseen tensor (Fig. 6). As shown, a Gaussian force field with the standard deviations of 2.6 μm along and 1.2 μm perpendicular to the vertical pump direction [Fig. 6(a)] fitted the measured flow [Fig. 6(b)]. Since scan patterns can be combined, we can generate almost arbitrary solutions of the two-dimensional Navier–Stokes equation with a similar resolution (see supplementary movies).[20] No other method that we know of can drive such arbitrary solutions of the Navier–Stokes equation.

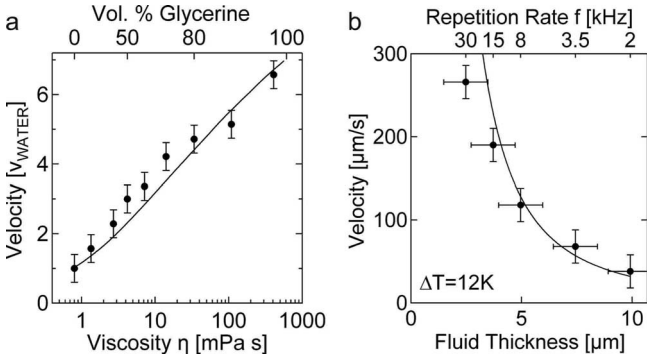

FIG. 7. Methods to enhance the pump speed. (a) Viscous fluids are pumped equally well, shown for viscous water-glycerol mixtures. The increased pump speed is the result of an increased β at a rising glycerol concentration. The parallel increase in viscosity does not quench pump velocities. (b) Pump speeds also increase for thinner chambers since the repetition rate f can be enhanced quadratically with decreasing chamber thickness.

G. Toward light driven nanofluidics

Highly viscous fluids can be pumped equally well and in many cases yield a considerably faster pump speed. For example, by adding glycerol to water, the pump speed increases 7-fold at a constant spot temperature despite a 500-fold increase in the viscosity [Fig. 7(a)]. This is the result of the increase in $|\alpha \cdot \beta|$ as predicted by Eq. (8), shown as solid line. Since thermoviscous pumping in 10 μm thin water is four to five orders of magnitude away from the pressure limitation of typical microfluidic chambers, pumping liquids of even higher viscosities or in thinner chambers is possible without reduced pump velocity. Due to the local pumping mechanism, problems from large viscosity or thin chambers are much less an issue for the described light driven flow as compared to classical pressure driven microfluidics.

The thermal relaxation time τ of the cooling is provided by the chamber walls and significantly depends on the chamber height. In sufficiently thin chambers, the heat flow is predominantly perpendicular to the fluid film and the temperature dynamics can be approximated with a single exponential decay of one-dimensional diffusion with a time constant of $\tau = d^2/(\pi^2 \kappa)$ where d denotes the fluid thickness and κ the thermal diffusivity. Therefore, the warm spot retains its circular shape if the repetition frequency is scaled according to $f \propto 1/d^2$. As a consequence, the pump speed becomes quadratically faster for thinner chambers. This dependence was tested experimentally in Fig. 7(b). We varied the chamber thickness and adjusted the repetition frequency accordingly. The temperature profile of the spot remained constant with $b = 19$ μm. This was checked independently with fluorescence imaging of the spot temperature (not shown). The small deviations for thinner chambers probably can be assigned to speed limitations of the used acousto-optical laser deflector. As estimated before, pressure should not limit pumping fluids at the nanoscale, even for fluids with increased viscosity. In the experiment, the decreased light absorption by thinner fluid films was compensated by increased

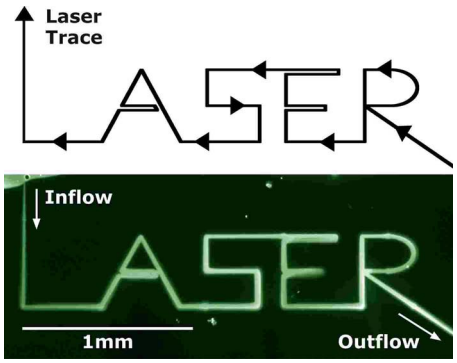

FIG. 8. (Color online) Millimeter-scale unidirectional flow of beads with 20 nm diameter along the letters "LASER." The laser focus guides the fluid with the beads through a low melting agarose gel from an aqueous reservoir on the top left through a gel and back into the aqueous reservoir on the right side of the image.

laser power. The latter poses no fundamental limitation since the light can be alternatively absorbed by nanoscale metal films on the chamber walls.

H. Light driven microfluidics in 2D fluid films

While the dynamic control of fluid flow on the micrometer scale is an interesting subject by itself, the capability to transport dissolved molecules is crucial for microfluidic applications. Traditional microfluidics use micromachined channels to hinder diffusion of molecules perpendicular to the pump direction. While our technique can also pump along such optically transparent channels, we aim at more flexible and previously impossible settings. For example, the method allows the usage of unstructured and disposable chambers. In the following, microfluidic experiments were performed by sandwiching microliter-scale fluid droplets between two microscope cover slips. We demonstrate the millimeter-scale transport of nanoparticles and the aliquotation and mixing for short DNA.

First, we pumped fast diffusing 20 nm fluorescent beads across several millimeters in a gel along the letters "LASER" (Fig. 8). The initial condition was prepared by sandwiching two droplets between glass slides: one drop contained the beads in water and the other drop initially warm low melting temperature agarose gel. At the interface, the beads were pumped into the gel which was liquefied by the heating and replaced by the bead-water solution. The gel effectively reduced lateral diffusion and allowed the microscale definition of pump channels (Fig. 8). For the future, besides using gels to hinder diffusion, the optical creation of pump paths by melting thin ice sheets appears to be a useful approach.

I. Light driven aliquotation of DNA

To show how light driven pumping can be used in microfluidic applications, we demonstrate a purely light driven fluid mixer for small biomolecules (Fig. 9). Two geometries are presented. In the first geometry, the fluorescent molecules are pumped into three pockets of different areas and mixed with the surrounding dark liquid with volume ratios of 4:1, 1:1, and 1:4 [Fig. 9(a)]. Secondly, a geometry for faster mixing into a larger number of pockets is shown in Fig. 9(b).

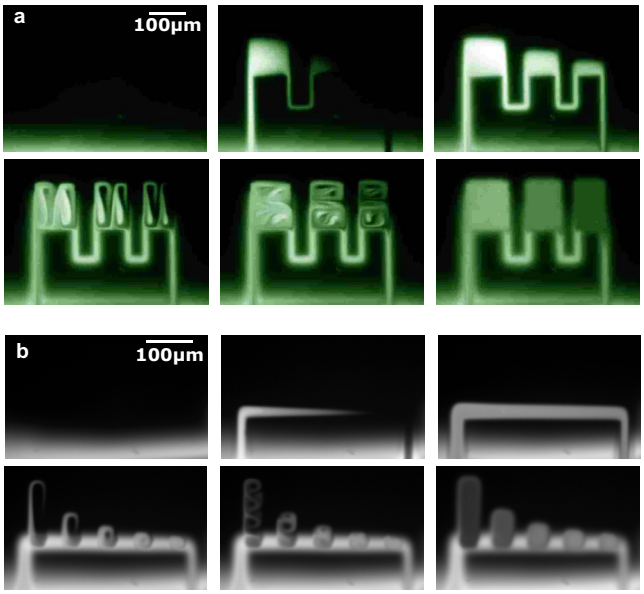

FIG. 9. (Color online) Light driven mixing of DNA hairpins in dynamically created gel pockets. (a) Two liquids are mixed with different ratios simultaneously. Fluorescein-Dextran (MW 40.000) is pumped from a liquid boundary (bottom) into three chambers of different size. It is mixed with the dye-free liquid (top) in equally sized areas at volume mixing ratios of 4:1, 1:1, and 1:4. The mixing is performed all optically without any microfluidic walls and without any contact to the liquid other than the unstructured cover slips that border the fluid film. At the used repetition frequency $f=120$ Hz the mixing sequence took 280 s. (b) A 40-base DNA Hairpin (bottom, bright) is mixed with target DNA (top, dark) at mixing ratios 1:8, 1:4, 1:3, 1:2, and 1:1. The mixing is provided from a single channel into pockets of variable size. The overall mixing time is 170 s at $f=140$ Hz. The corresponding movies are supplied as supplementary material.

From an initial channel along a straight line, a 40 base DNA hairpin (molecular beacon) is mixed with target DNA with the ratios 1:8, 1:4, 1:3, 1:2, and 1:1. Depending on the target DNA concentration, the hairpin opens up and changes the fluorescence signal. The time required for the latter mixing protocol is 170 s. In the next paragraph we present a tailored chamber material which enhances the protocol speed by more than a factor of 10.

J. Enhanced speed using light absorption layer

The repetition frequency of $f=100$ Hz used in the mixing experiments of Fig. 9 was very moderate and could be raised at least 20-fold to 2 kHz which would increase the pump speed considerably as seen in Fig. 2(b). To achieve this, we switched to a more elaborate chamber wall material with enhanced thermal conduction and a light absorbing layer at the solid-water interface. We used a 40 nm thin CrNi film on a double-sided polished silicon wafer to absorb 30% of the laser light. The enhanced power deposition is used to achieve faster repetition rates at the same spot temperatures. The resulting aliquotation and mixing experiment is shown in Fig. 10. A dilution series of biomolecules is achieved within 15 s. As before, aliquots of one liquid were first created by pumping defined volumes across a gel interface. Three chambers in the gel with different volumes (65, 40, and 20 pl) were formed. In the second step the fluid was mixed with the surrounding fluid to obtain equal volumes of 80 pl. Efficient mixing was accomplished by repeatedly

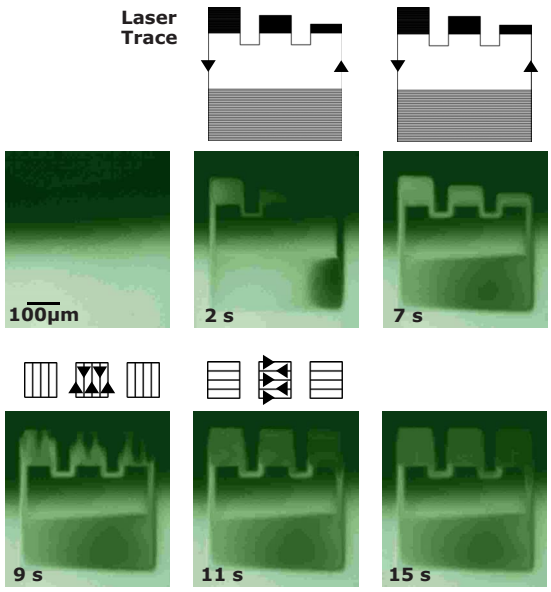

FIG. 10. (Color online) Fast light driven creation of a dilution series. Biomolecules are aliquoted and mixed from an interface of two neighboring gels. First, three volumes of 65, 40, and 20 pl are created. In a second step the fluid is mixed by repeatedly pumping rectangular ring flows with perpendicular orientation. The result is a dilution series with volume ratios of 4:1, 1:1, and 1:4 in equal volumes. Due to the light absorbing chamber wall composite material, protocol time drops to 15 s. The corresponding movie can be found in the supplementary materials section.

pumping rectangular ring flows with perpendicular orientation (see inset in Fig. 10). The resulting dilution series had final volume ratios of 4:1, 1:1, and 1:4. This example demonstrates the speed and flexibility by applying different pump patterns over time.

K. Possibilities and limitations

Light driven pumping reaches velocities of up to 150 μm/s for moderate heating. In comparison, pressure driven microfluidics typically operate with tenfold faster flow speeds. However, these fast speeds need millimeter-sized interfacial connections to outside pumps. The presented method allows for highly localized fluid actuation. We imagine to apply fluid volumes locally, for example, by spotting droplets onto inlets in close proximity of the gel. It is also possible to place ice pads near a two-dimensional ice sheet in which the light driven pumping would be performed. We want to note that adding glass formers to the solution increases the pump speed by raising the parameters α and β. For example, the glycerine-water mixture was pumped up to sixfold faster at equal spot temperature as shown in Fig. 7(a). More specialized glass formers with stronger effects are likely to exist and could be used to increase the speed of pumping considerably.

As the pump pattern is programmable in real time, pumping can be adapted to varying geometries. For example, living cells produce minute amounts of intracellular signals. Thermoviscous pumping could selectively enhance the transport of these signalling molecules from one cell to another with pump paths that are adapted in real time to the positions of the cells. Also, the pumping mechanism is not limited to be driven by optical means. Heating from a wide variety of other sources such as electrical currents will equally pump fluids, extending previously explored electrical movement strategies using electrophoresis[23] or surface acoustic waves.[24] However, the physical isolation between the light source used as fluid actuator and the chamber comprising the fluid will allow to pump inside complex chambers hosting extreme fluid pressures or temperatures. The temperature gradients that are imposed by the pump mechanism can be combined with thermophoretic effects which move molecules along a temperature gradient.[19,25] For example, thermophoretic traps for biomolecules simulating hydrothermal conditions[26,27] should become feasible at much smaller length scales, enabling fast equilibration times. Finally we want to note that pumping in three dimensions should be achievable with highly focused heating of the fluid or even two-photon heating using adequate dyes.

IV. CONCLUSIONS

We found a physical mechanism to pump liquids along arbitrary geometries with a laser scanning microscope. The fluid flow follows the movement of a warm heating spot that is created optically by light absorption. Arbitrary flow patterns can be realized with path widths close to the optical resolution. The mechanism is based on the thermal expansion in a viscosity gradient in the vicinity of a moving warm spot. This optical pumping has the potential to complement microfluidic designs with valveless, contactless, and pumpless flow at the micrometer and submicrometer scales. Supplementary information accompanies the paper.

ACKNOWLEDGMENTS

We thank Joseph Egger for help in solving the fluid dynamics, Jonas A. Kraus and Thomas Franosch for discussions, Philipp Baaske and Ingmar Schön for reading the manuscript, Klaus Stierstadt for comments, Stefan Duhr and Ingmar Schön for assistance, and Hermann Gaub for hosting our Emmy-Noether Group. This work was funded by the Emmy Noether Program of the Deutsche Forschungsgemeinschaft (DFG) and supported by the Center for Nanoscience Munich (CENS) and the Nanosystems Initiative Munich (nim).

[1] D. J. Harrison, K. Fluri, K. Seiler, Z. Fan, C. S. Effenhauser, and A. Manz, Science **261**, 895 (1993).
[2] B. H. Weigl, Science **283**, 346 (1999).
[3] T. Thorsen, S. J. Maerkl, and S. R. Quake, Science **298**, 580 (2002).
[4] J. Tian, H. Gong, N. Sheng, X. Zhou, E. Gulari, X. Gao, and G. Church, Nature (London) **432**, 1050 (2004).
[5] T. M. Squires and S. R. Quake, Rev. Mod. Phys. **77**, 977 (2005).
[6] R. B. M. Schasfoort, S. Schlautmann, J. Hendrikse, and A. van den Berg, Science **286**, 942 (1999).
[7] B. Zhao, J. S. Moore, and D. J. Beebe, Science **291**, 1023 (2001).
[8] B. S. Gallardo, V. K. Gupta, F. D. Eagerton, L. I. Jong, V. S. Craig, R. R. Shah, and N. L. Abbott, Science **283**, 57 (1999).
[9] M. G. Pollack, R. B. Fair, and A. D. Shenderov, Appl. Phys. Lett. **77**, 1725 (2000).
[10] D. Psaltis, S. R. Quake, and C. Yang, Nature (London) **442**, 381 (2006).
[11] P. Y. Chiou, Z. Chang, and M. C. Wu, Proceedings of the Micro Electro Mechanical Systems, 2003 (unpublished), p. 355.
[12] P. Y. Chiou, A. T. Ohta, and M. C. Wu, Proc. SPIE **5514**, 73 (2004).
[13] K. Ladavac and D. Grier, Opt. Express **12**, 1144 (2004).
[14] A. A. Darhuber, J. M. Davis, S. M. Troian, and W. W. Reisner, Phys.

Fluids **15**, 1295 (2003).
[15]A. Wixforth, C. Strobl, C. Gauer, A. Toegl, J. Scriba, and Z. v. Guttenberg, Anal. Bioanal. Chem. **379**, 982 (2004).
[16]A. Ashkin, Phys. Rev. Lett. **24**, 156 (1970).
[17]A. Ashkin, Proc. Natl. Acad. Sci. U.S.A. **94**, 4853 (1997).
[18]S. M. Block, L. S. B. Goldstein, and B. J. Schnapp, Nature (London) **348**, 348 (1990).
[19]S. Duhr and D. Braun, Proc. Natl. Acad. Sci. U.S.A. **103**, 19678 (2006).
[20]See Document No. E-JAPIAU-104-001823 for supplementary movies and Femlab 3.1 simulation files. For more information on EPAPS, see http://www.aip.org/pubservs/epaps.html.
[21]E. Yariv and H. Brenner, Phys. Fluids **16**, L95 (2004).
[22]F. M. Weinert, J. A. Kraus, T. Franosch, and D. Braun, Phys. Rev. Lett.**100**, 164501 (2008).
[23]A. Ros, R. Eichhorn, J. Regtmeier, T. T. Duong, P. Reimann, and D. Anselmetti, Nature (London) **436**, 928 (2005).
[24]Z. Guttenberg, H. Müller, H. Habermüller, A. Geisbauer, J. Pipper, J. Felbel, M. Kielpinski, J. Scriba, and A. Wixforth, Lab Chip **5**, 308 (2005).
[25]C. Ludwig, Sitzungsber. Akad. Wiss. Wien, Math.-Naturwiss. Kl. **20**, 539 (1856).
[26]P. Baaske, F. M. Weinert, S. Duhr,K. H. Lemke,M. J. Russell, and D. Braun, Proc. Natl. Acad. Sci. U.S.A. **104**, 9346 (2007).
[27]D. Braun and A. Libchaber, Phys. Rev. Lett. **89**, 188103 (2002).